DesignCon 2018

A Causal Conductor Roughness Model and its Effect on Transmission Line Characteristics

Vladimir Dmitriev-Zdorov, Mentor Graphics, A Siemens Business,
vladimir_dmitriev-zdorov@mentor.com

Bert Simonovich, Lamsim Enterprises Inc.,
lsimonovich@lamsimenterprises.com

Igor Kochikov, Mentor Graphics, A Siemens Business,
igor_kochikov@mentor.com

Abstract

In the GB/s regime, accurate modeling of insertion loss and phase delay is a precursor to successful high-speed serial link designs. We propose a causal (physically meaningful) form of the Hammerstad and Cannonball-Huray metal roughness frequency dependent complex correction factor. Compared to the widely used, non-causal form, it considerably increases the inductive component of internal metal impedance. Transmission lines simulated with a causal version demonstrate increased phase delay, and characteristic impedance. By obtaining the dielectric and roughness parameters, solely from manufacturers' data sheets, we validate the model through a detailed case study to test the model`s accuracy.

Author(s) Biography

Dr. Vladimir Dmitriev-Zdorov is a principal engineer at Mentor Graphics Corporation. He has developed a number of advanced models and novel simulation methods used in the company's products. His current work includes development of efficient methods of circuit/system simulation in the time and frequency domains, transformation and analysis of multi-port systems, and statistical and time-domain analysis of SERDES links. He received Ph.D. and D.Sc. degrees (1986, 1998) based on his work on circuit and system simulation methods. The results have been published in numerous papers and conference proceedings.

Bert Simonovich graduated from Mohawk College of Applied Arts and Technology, Hamilton, Ontario Canada, as an Electronic Engineering Technologist. Over a 32-year career, working at Bell Northern Research/Nortel, in Ottawa, Canada, he helped pioneer several advanced technology solutions into products. He has held a variety of engineering, research and development positions, eventually specializing in high-speed signal integrity and backplane architectures. After leaving Nortel in 2009, he founded Lamsim Enterprises Inc., where he continues to provide innovative signal integrity and backplane solutions as a consultant. He has also authored and coauthored several publications; posted on his web site at www.lamsimenterprises.com. His current research interests include: high-speed signal integrity, modeling and characterization of high-speed serial link architectures.

Dr. Igor Kochikov received his PhD degree in computational mathematics from Moscow State University in 1985. Since 1998 with Mentor Graphics, focusing on PCB and interconnect electromagnetic modeling, providing software architecture definition and development of the fast and reliable simulation methods in signal integrity and power integrity applications. He has also been involved in computer-aided research in various fields of physics and authored several books and numerous papers in physical chemistry, optics, spectroscopy and molecular structural analysis.

Introduction

Metal loss is an increasingly important factor affecting design quality in all high-speed applications. As operational frequencies went up, it became evident that formulas ignoring roughness of the metal surface greatly underestimated losses. A number of approaches have been proposed over the years [1-3] that introduced additional losses by applying frequency-dependent correction to the impedance of the smooth metal. Recent survey in this area can be found in [4].

As of today, a widely accepted approach to model an impedance of the rough metal is taking a complex frequency-dependent impedance of the smooth metal and applying to it a multiplier $K(\omega)$ that monotonically grows from 1 to $K(\infty)>1$. Virtually all publications on this topic and a vast majority of commercially available simulators assume that this correcting multiplier is a real-value function. In the literature, it is often called "roughness correction factor".

Since the internal impedance of the smooth surface is described by the well-known "skin effect" formula, where real and imaginary parts of the impedance are equal, applying a real multiplier to it obviously produces the complex value where the parts (resistive and inductive components of impedance) are also equal. For example, [2-4] give us the following relations: $R_{ac}(\omega) = K(\omega)\sqrt{\omega}R_s$, $L_{\text{int}}(\omega) = R_{ac}(\omega)/\omega$, making $R_{ac}(\omega)$ and $\omega L_{\text{int}}(\omega)$ definitely equal. Similar equations/statements can be found in many other publications, including major textbooks.

Is this a physically valid model of metal impedance? Can we apply a frequency-dependent real multiplier to a causal dependence, which the smooth impedance formula definitely is, without violating causality? There are only few sources known to us that have raised these questions.

First, this issue was addressed in [5] where the authors mention that inductive and resistive portion of the metal's internal impedance are generally not equal, but should be mutually related by Hilbert transform to enforce model causality. Indeed, the roughness correction factor $K(\omega)$ was defined and derived as a ratio of the active power dissipated on a rough metal to that dissipated on a perfectly smooth metal. From here, it follows that it describes proportionality between the resistive portions of the impedance only. As to wording, it would make sense to call $K(\omega)$ a "loss correction factor" because we have no evident reasons to believe that inductive component should be increased in the same proportion. Another publication [6] actually applied this idea to find a causal version of Huray's roughness formula.

It's remarkable that these results, despite laying a perfect ground for building physically meaningful causal models of metal roughness, went majorly unnoticed. Hence the commonly used practice hasn't changed since then. Perhaps, this can be explained by the fact that [5] did not provide practical examples of causal versions of known models, while [6] might appear too academic to the readers, and possibly didn't contain enough evidence that would convince them to immediately start using the causal model.

A far-reaching goal of this paper is to give an additional impetus to this development and make causal roughness models part of the mainstream paradigm when simulating metal losses. As we remember, this happened a few years ago with the introduction of causal dielectric loss modeling [7, 8]. Now is the time for the metal.

In addition, we would like to fill in some knowledge gaps regarding this subject, such as:

- General approach to derivation of causal models from given analytical expression (or another reasonably complete description) of the metal loss correction factor.
- Basic relationships existing between loss correction factor, inductance correction factor, complex correction factor, real and imaginary parts of internal impedance and inductance of the rough metal.
- Side-by-side comparison of those dependences between causal and non-causal versions of Hammerstad and Cannonball-Huray models.
- Derivation of causal roughness model from loss correction factor specified as tabulated dependence.

We also show that:

- As necessitated by causality requirements, inductive portion of the internal metal impedance of the rough metal is not equal, but appears much larger than the corresponding resistive portion of it.
- We analyze the effect of using a causal model of metal roughness on the characteristics of transmission lines. Under other conditions being equal, a causal model makes the line's delay and characteristic impedance larger than with non-causal models. We provide expressions which formally evaluate this difference.
- We compare measured characteristics of stripline to simulations when using causal and non-causal versions of the Cannonball-Huray roughness model [11]. The Cannonball-Huray model is a simple model, based on cubic close-packing of equal spheres, which can be used to determine the sphere radius and area parameters for the Huray roughness formula. The cannonball stack is an example of a cubic close-packing of equal spheres, thus the name for the model. By obtaining published conductor roughness parameters, solely from manufacturers' data sheets, the model has shown excellent agreement to measured results up to 50 GHz.

This paper is organized as follows: Section I gives general relationships for the causal roughness correction multiplier, and outlines the process of deriving a causal correction factor for a given analytical expression for the loss correction coefficient. In Section II we apply this approach to Cannonball-Huray and Hammerstad models. Section III analyzes the results for Cannonball-Huray and Hammerstad models. In Section IV, we evaluate the effect of using causal models when analyzing lossy transmission lines. In Section V we outline the process of finding a complex causal model when the loss correction factor is given by a table. In Section VI, we describe the Cannonball-Huray roughness model in more detail. Then, we validate the model,

through a case study, using causal and non-causal versions of Cannonball-Huray formula and compare them to the measured results.

I. General relationships

As shown in [2, 3], an internal impedance of the metal with smooth surface is related to the skin depth, an effective penetration of electromagnetic field into metal surface:

$$\delta(f) = \frac{1}{\sqrt{\pi f \mu_0 \sigma}} \tag{1}$$

where f is frequency (Hz), μ_0 is permeability of free space (H/m) and σ is metal conductivity (S/m). As follows from this formula, the thickness of the effective conducting layer decreases as $1/\sqrt{f}$, thus causing an increase in metal impedance in inverse proportion. From here it follows a well-known formula for the complex impedance of the smooth conductor: $Z_{smooth}(i\omega) = (1+i)\sqrt{\omega} R_{s\omega}$, which we will slightly modify and represent as a function of the normalized frequency x:

$$Z_{smooth}(ix) = (1+i)\sqrt{x} R_s = \sqrt{2s} R_s . \tag{2}$$

Here R_s is a "skin resistance", a constant factor that absorbs some material and geometrical parameters of the conductor, and $s = ix$ is a complex frequency. It is convenient to establish proportionality between the normalized frequency x and the angular frequency ω individually for each type of metal roughness model, and we will select it later. An impedance of the rough metal surface, under other conditions being equal, is larger and therefore can be expressed as

$$Z_{rough}(ix) = Z_{smooth}(ix) + Z_0(ix) \tag{3}$$

where $Z_0(ix)$ is an additional impedance due to metal roughness. As stated in [5], total and additional impedance caused by metal roughness must be a causal function, so that $\mathrm{Re}\, Z_0(s)$ and $\mathrm{Im}\, Z_0(s)$ must be mutual Hilbert transforms. In [1] and in many other sources, the loss correction factor is defined as a ratio of the power dissipated in a rough metal to that dissipated in a perfectly smooth metal. From this definition it follows that loss correction factor $k(x)$, a real function of frequency, is also the ratio of the resistive part of impedance of rough metal to the resistive part of impedance of smooth metal:

$$k(x) = \mathrm{Re}\, Z_{rough}(ix) / \mathrm{Re}\, Z_{smooth}(ix) = 1 + \mathrm{Re}\, Z_0(ix) / \mathrm{Re}\, Z_{smooth}(ix) = 1 + k_0(x) . \tag{4}$$

In all practical cases it is assumed that $k_0(0) = 0$, because metal roughness makes no addition to impedance at low frequency.

Note that it would be improper to use the relations $Z_{rough}(x) = k(x)Z_{smooth}(ix)$ or $Z_0(x) = k_0(x)Z_{smooth}(ix)$, because we have no evidence that roughness modifies inductive (imaginary) part of impedance in the same proportion as it does for resistive (real) part. Instead, we should assume that there exists similar relationship with complex (yet unknown) factor $K_0(ix)$:

$$Z_0(ix) = K_0(ix)Z_{smooth}(ix). \tag{5}$$

How can we practically find $K_0(ix)$? From (2) and (4), it follows that:

$$\mathrm{Re}\, Z_0(ix) = k_0(x)\,\mathrm{Re}\, Z_{smooth}(ix) = k_0(x)\sqrt{x}R_s \tag{6}$$

and we also know that $Z_0(ix)$ must be a causal function. For causal complex function, imaginary part can be restored from known real part (6), by using certain types of Kronig-Kramers (K-K) relations. Once the missing imaginary part $\mathrm{Im}\, Z_0(ix)$ is restored, the unknown complex correction factor can be found as:

$$K_0(ix) = Z_0(ix) / Z_{smooth}(ix). \tag{7}$$

With known causal complex correction factor, an additional impedance due to metal roughness becomes:

$$Z_0(s) = K_0(s)\sqrt{2s}R_s. \tag{8}$$

From (8), we can express the factors at real and imaginary parts of the impedance of smooth metal as:

$$Z_0(s) = Z_{0r}(x) + iZ_{0i}(x) = K_0(ix)(1+i)\sqrt{x}R_s =$$

$$[K_{0r}(x) - K_{0i}(x)]\sqrt{x}R_s + i[K_{0r}(x) + K_{0i}(x)]\sqrt{x}R_s. \tag{9}$$

As we see, real and imaginary parts of skin impedance are increased by different factors. The one in the real part describes *loss correction factor*, the other is an *inductance correction factor*. Also, comparing (4) and (9), we see that

$$[K_{0r}(x) - K_{0i}(x)] = k_0(x). \tag{10}$$

This result matches [6]. An important conclusion from here is that for a given complex correction factor that applies to complex impedance of the smooth metal, the loss correction factor is a difference between its real and imaginary parts, whereas an inductance correction factor is a sum of real and imaginary parts of the same complex factor. As we see, metal roughness modifies resistive and inductive parts of the smooth metal in different proportion.

Below, we will also need an expression for an additional complex inductance caused by metal roughness. It can be found as a ratio of the complex impedance (8) and complex frequency as $L_0(s) = Z_0(s)/s = K_0(s)\sqrt{\frac{2}{s}}R_s$. Real and imaginary parts of the complex impedance and inductance are related as $L_0(ix) = L_{0r}(x) + iL_{0i}(x) = Z_{0i}(x)/x - iZ_{0r}(x)/x$. Therefore, imaginary part of the inductance can be found as

$$L_{0i}(x) = -Z_{0r}(x)/x = -(k_0(x)\sqrt{x}R_s)/x = -\frac{k_0(x)}{\sqrt{x}}R_s \ . \tag{11}$$

As we see, it is fully defined by the loss correction factor.

II. Finding causal correction factor for Cannonball-Huray and Hammerstad models

Cannonball-Huray model

We will use the above equations to illustrate the process of deriving complex correction factor for a single component of the Cannonball-Huray roughness model. As shown in [3, 11], these models define loss correction factor in a form of the sum

$$K_{sph}(f) = A_0 + \sum_{n=1}^{N} \frac{A_n}{1 + \frac{\delta(f)}{a_n} + \frac{\delta^2(f)}{2a_n^2}} \tag{12}$$

where $\delta(f)$ is a skin depth defined in (1), a_n are radii of spherical shapes representing rough metal, and factors A_n are constant and defined by geometry assumed by each model.

Let's consider n-th summand in (12), assuming $A_n = 1$. By introducing a dimensionless normalized frequency $x = \left(\sqrt{2}a_n/\delta(f)\right)^2 = \omega\mu_0\sigma a_n^2$, we represent this component as a simple function of a single argument:

$$k_0(x) = \frac{1}{1 + \sqrt{2/x} + 1/x} = \frac{x}{x + \sqrt{2x} + 1}, \ x > 0 \, . \tag{13}$$

Then, using definitions and ideas from Section I, we derive a complex factor as shown in Appendix A. This factor becomes $K_0(ix) = \frac{\sqrt{ix}}{1 + \sqrt{ix}}$. Considering all summands in (12), the final result becomes:

$$K_{sph}(if) = A_0 + \sum_{n=1}^{N} \frac{A_n \sqrt{ix_n}}{1+\sqrt{ix_n}} \text{ , where } x_n = 2\pi f \mu_0 \sigma a_n^2 . \quad (14)$$

Hammerstad model

Hammerstad loss correction factor [2] is given by equation:

$$K_{hmst}(f) = 1 + A_1 \frac{2}{\pi} \arctan(1.4(\Delta / \delta(f))^2) \quad (15)$$

where Δ is r.m.s. surface roughness, and $\delta(f)$ is skin depth. The normalized offset-free factor here is

$$k_0(x) = \frac{2}{\pi} \arctan(x), \text{ where } x = 1.4\pi f \mu_0 \sigma \Delta^2 . \quad (16)$$

Derivation of the complex correction factor can be found in Appendix B. The resulted causal factor becomes:

$$K_{hmst}(if) = 1 + (A_1 / \pi)[\log \frac{1+\sqrt{s}}{1-\sqrt{s}} - \log \frac{1+s}{1-s} + 2\arctan(\sqrt{s})] \quad (17)$$

where $s = ix$ is complex frequency, and x is defined in (16).

III. Causal versions of Hammerstad and Cannonball-Huray roughness models

The approach we outlined in previous section can be applied to any other model type, if the loss correction factor is represented by a continuous analytical function. Some details could be different though, such as variable techniques when finding K-K integral.

In this section we present formal results for causal and non-causal versions of Hammerstad and Cannonball-Huray models. To allow side-by-side comparison, we put formulas into Table 1 below. For completeness, the table contains definition of smooth metal impedance, and normalized frequencies used in each case.

As we see, complex characteristics, such as normalized complex correction factor, impedance and inductance added due to metal roughness, are functions in complex frequency. There exist inverse Laplace transforms of these characteristics, thus proving their causality. At the same time, these models provide loss increase factor (#2 in the Table 1), exactly as defined for the corresponding model types.

Table 1. Formulas describing causal Hammerstad and Cannonball-Huray models

	Causal Models	Hammerstad	Cannonball-Huray
	Impedance of smooth metal $Z_{smooth}(s)$, where $s = ix$	$R_s(\sqrt{x} + i\sqrt{x}) = \sqrt{2ix}R_s = \sqrt{2s}R_s$	
	Additional impedance due to metal roughness	$K_0(s)\sqrt{2s}R_s$	
1	Normalized frequency x	$1.4\pi f\mu_0\sigma\Delta^2$, Δ is r.m.s. surface roughness	$\omega\mu_0\sigma a^2$, a is a ball radius
2	Normalized loss increase factor $k_0(x)$	$\frac{2}{\pi}\arctan(x)$	$\frac{x}{x+\sqrt{2x}+1}$
3	Normalized complex correction factor $K_0(s)$	$\frac{1}{\pi}[\log\frac{1+\sqrt{s}}{1-\sqrt{s}} - \log\frac{1+s}{1-s} + 2\arctan(\sqrt{s})]$	$\frac{\sqrt{s}}{1+\sqrt{s}}$
4	$K_{0r}(x)$, real part of $K_0(ix)$	$\frac{1}{\pi}\left[\frac{1}{2}\log\frac{1+\sqrt{2x}+x}{1-\sqrt{2x}+x} + \arctan\frac{\sqrt{2x}}{1-x}\right]$ (*1)	$\frac{x+\sqrt{x/2}}{x+\sqrt{2x}+1}$
5	$K_{0i}(x)$, imaginary part of $K_0(ix)$	$\frac{1}{\pi}\left[\frac{1}{2}\log\frac{1+\sqrt{2x}+x}{1-\sqrt{2x}+x} + \arctan\frac{\sqrt{2x}}{1-x} - 2\arctan(x)\right]$	$\frac{\sqrt{x/2}}{x+\sqrt{2x}+1}$
6	$K_{0r}(x) - K_{0i}(x)$, Loss increase factor: a factor at smooth metal resistance, making an additional contribution into resistive part of impedance due to roughness	$\frac{2}{\pi}\arctan(x)$	$\frac{x}{x+\sqrt{2x}+1}$
7	$K_{0r}(x) + K_{0i}(x)$, Inductance increase factor: a factor at smooth metal inductance, making an additional contribution into inductive part of impedance due to roughness	$\frac{1}{\pi}\left[\log\frac{1+\sqrt{2x}+x}{1-\sqrt{2x}+x} + 2\arctan\frac{\sqrt{2x}}{1-x} - 2\arctan(x)\right]$	$\frac{x+\sqrt{2x}}{x+\sqrt{2x}+1}$
8	Complex impedance added due to metal roughness, normalized on R_s	$\frac{\sqrt{2s}}{\pi}[\log\frac{1+\sqrt{s}}{1-\sqrt{s}} - \log\frac{1+s}{1-s} + 2\arctan(\sqrt{s})]$	$\frac{\sqrt{2}s}{1+\sqrt{s}}$
9	Complex inductance added due to metal roughness, normalized on R_s	$\frac{\sqrt{2}}{\pi\sqrt{s}}[\log\frac{1+\sqrt{s}}{1-\sqrt{s}} - \log\frac{1+s}{1-s} + 2\arctan(\sqrt{s})]$	$\frac{\sqrt{2}}{1+\sqrt{s}}$

Note [*1]: To avoid discontinuity, here and below, $\arctan\frac{\sqrt{2x}}{1-x}$ should be computed as ATAN2($\sqrt{2x}$, $1-x$).

Let us now analyze these results side-by-side. In the plots below, characteristics of Hammerstad model are shown by dashed lines, while Cannonball-Huray model are shown by solid lines. If the plot provides real and imaginary parts of the dependence, they will be shown by red and blue color respectively. By [#n], we denote its position in Table 1.

In this section we intentionally consider the functions in normalized frequency, even though the exact definition of the normalized frequency in both cases is different. The functions may also have different multipliers. If the difference were only due to scaling/ normalization, it would be possible to overlap the curves on the logarithmic plots by shifting them along the axes. However, it is more than that, and we cannot make the curves coincide.

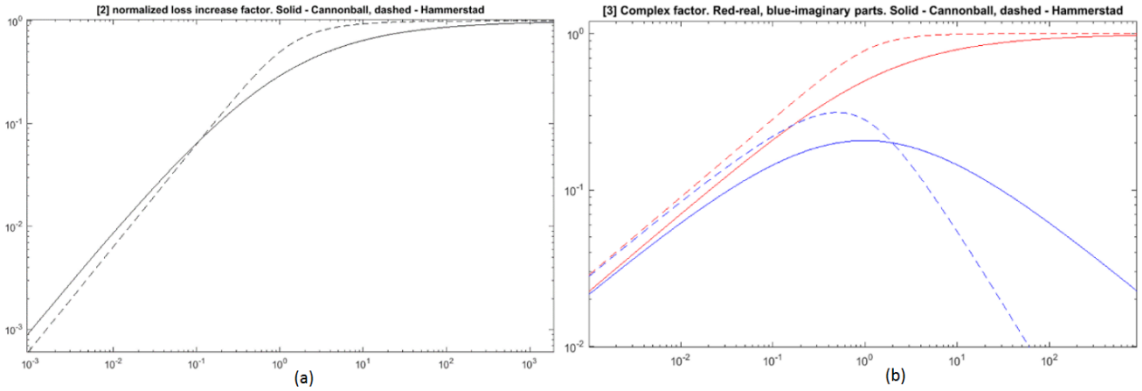

Figure 1. (a) Hammerstad and Cannonball-Huray loss correction factor [#2]; (b) real/imaginary parts of the complex correction factor [#4, #5]

The plots in Figure 1a are loss increase factors for the two models. Both have similar asymptotes; although Hammerstad model demonstrates steeper transition from linear grow to steady region.

Figure 1b shows real and imaginary parts of the complex correction factor. It helps to better understand the differences in the models' behavior. Real parts have similar asymptotes, at low and high frequencies, but imaginary parts don't. At low frequency the real and imaginary parts grow as $\sim\sqrt{x}$, but at high frequency, the imaginary part decreases as $\sim 1/\sqrt{x}$ for Cannonball-Huray, and $\sim 1/x$ for Hammerstad.

Limitations of the Hammerstad model become obvious when designers start to work at frequencies that correspond to the declining portion of the dependence. It turns out that the Hammerstad model settles too fast.

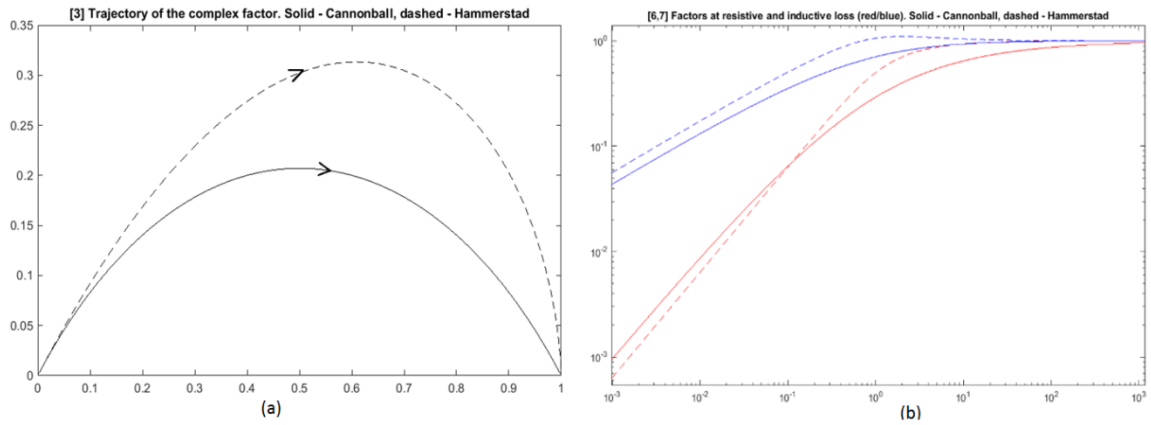

Figure 2. Trajectory plots representing complex factors [#3] over frequency range (a). Factors in resistive and inductive components of additional impedance, [#6] and [#7], (b)

Trajectories in Figure 2a illustrate the behavior of the complex correction factors over frequency. Note considerable asymmetry for the Hammerstad correction factor. It approaches saturation level much faster than Cannonball-Huray. The non-causal versions of both models, if plotted, would show a straight line segment along real axis, from 0 to 1.

Figure 2b shows multipliers (at skin impedance) creating additional resistive and inductive components due to roughness. Loss (resistive component) is defined by red curves [#6], same as original real correction factors [#2] in Figure 1. Blue curves [#7] show the factors that apply to inductance. At low frequency they grow as $\sim\sqrt{x}$ and considerably exceed resistive, which grow as $\sim x$. A non-causal model would make both factors equal [#2] (red) thus causing considerable underestimation of internal inductance.

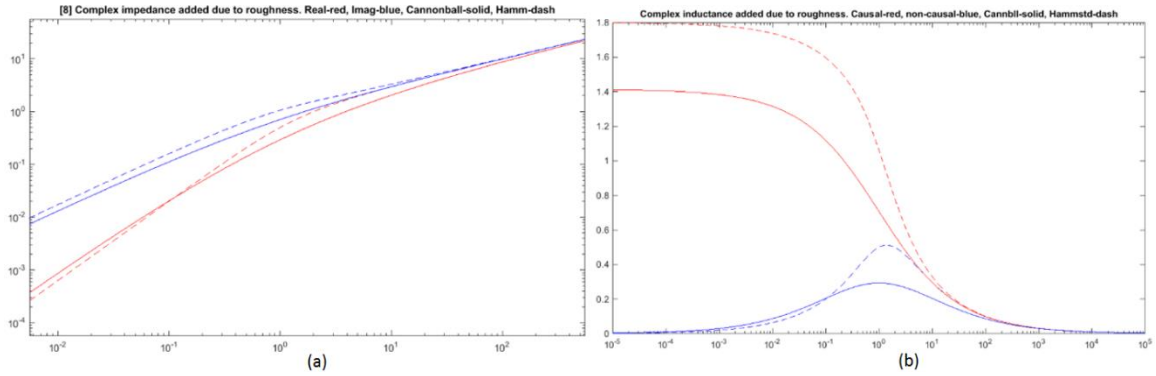

Figure 3. (a) Complex impedance contributed by metal roughness: resistive portion (red) and inductive (blue), [#8]. (b) An additional complex inductance, per [#9] in Table 1. For convenience, imaginary part of inductance is shown with opposite sign (as positive)

Figure 3a illustrates complex impedance added due to metal roughness. Resistive portion is shown in red, inductive shown in blue. In both cases the inductive component considerably

exceeds resistive. Non-causal version suggests that both are equal and coincide with red. Both models provide similar asymptotes at low and high frequency. At low frequency, the inductive part of impedance grows as $\sim x$, while the resistive part grows as $\sim x^{3/2}$. At high frequency they both grow as $\sim \sqrt{x}$. However, Cannonball-Huray dependences are smoother (solid lines).

Figure 3b shows complex inductance added due to metal roughness. It is what we used in K-K relations. Real part of inductance is shown by red, while imaginary part of inductance with opposite sign is shown in blue. Note that the negative imaginary part of inductance, after multiplication on complex frequency, becomes positive loss resistance. When using non-causal model, both real inductance and loss would coincide with blue curve making inductance to vanish at low frequency. To some extent, a dramatic deficiency of inductance in the non-causal model remained unnoticed, due to the fact that inductance doesn't produce large impedance at low frequency. Still, as we will show, this difference is noticeable and practically important.

So far, we have only considered additional impedance caused by metal roughness. This impedance corresponds to $Z_0(ix)$ in equation (3). But how significant is this contribution when impedance of the smooth metal is factored in?

Let us analyze $Z_{rough}(ix)$, which is an internal impedance of rough metal that includes both components. Here, however, we need to know one more parameter. When studying *addition* to impedance due to roughness, we assumed that the loss factor $k_0(x)$ in (4) is normalized, i.e. $\lim_{x\to\infty} k_0(x) = 1$. Now, let's consider $Z_{rough}(ix) = [1 + AK_0(ix)]Z_{smooth}(ix)$ with factors varied as $A = 1,2,4,8$.

The results are shown in Figure 4, (a)-(d). It is interesting that inductive and resistive components of the impedance in Figure 4 (a), (c) are not equal, and do not exactly behave as $\sim \sqrt{f}$. They do so only at very low and very high frequencies. But in the middle they have an inflection that happens at different frequencies for resistive and inductive components.

Also, as we can see in Figure 4 (b) and (d), even in the combined impedance, the ratio between inductive and resistive component is considerable and reaches factor 2-3.

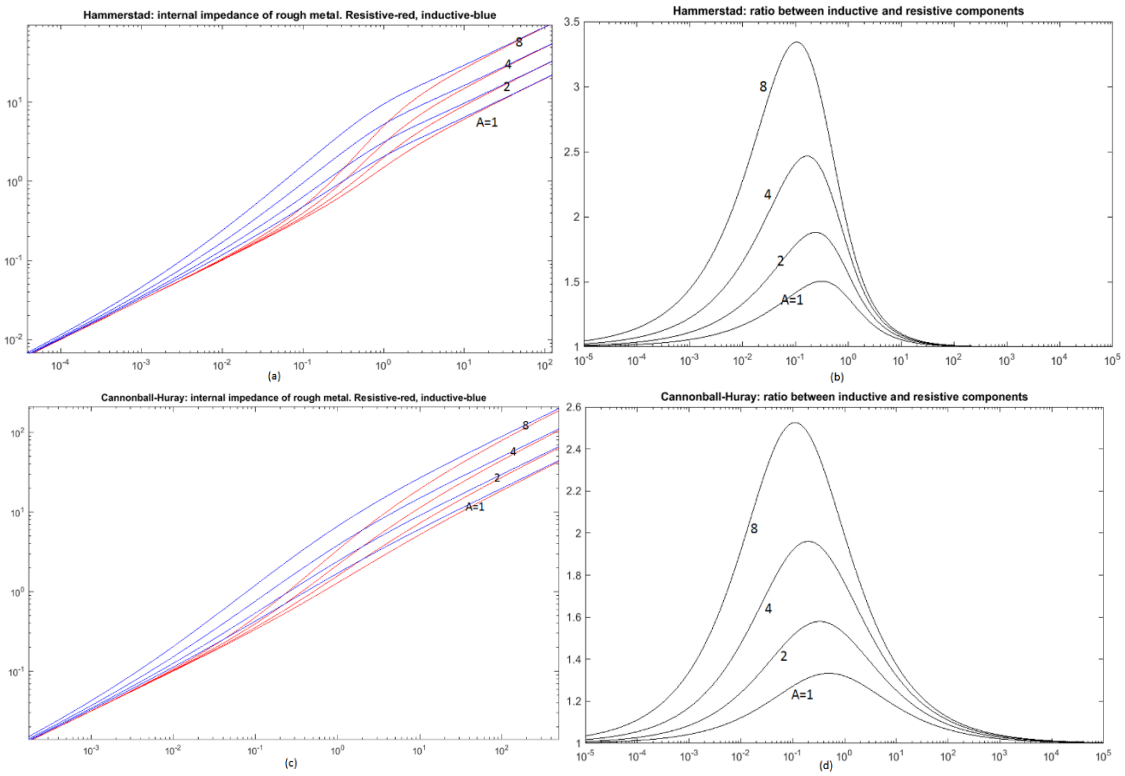

Figure 4. Skin impedance modified by roughness – left plots. Ratio of inductive component to resistive – right plots. First row corresponds to Hammerstad, second – to Cannonball-Huray

IV. Causal roughness models and characteristics of transmission lines

If we want to know how model causality, or non-causality, affects the characteristics of transmission lines, we need to consider more variables and parameters. In this section, we will assume that per-unit-length (PUL) parameters of the single-conductor transmission lines are known, and will evaluate the effect of using a causal model on a number of important characteristics, namely insertion loss, phase delay and characteristic impedance. This way, we will get general estimates of the error in a formal way.

We start from the line's propagation operator, and will try to simplify it, assuming that the resistive loss produces a smaller contribution than the inductive portion of impedance. Similarly, assume that dielectric loss produces a smaller conductance than that of the capacitance.

Therefore, the losses can be separated in the propagation operator as follows:

$$G(i\omega) = e^{-l\sqrt{(i\omega L + r(\omega))(i\omega C + g(\omega))}} = e^{-i\omega l\sqrt{LC}\sqrt{(1+\frac{r(\omega)}{i\omega L})(1+\frac{g(\omega)}{i\omega C})}} \approx e^{-i\omega l\sqrt{LC}[1+\frac{r(\omega)}{2i\omega L}+\frac{g(\omega)}{2i\omega C}]}. \qquad (18)$$

In (18) we assume that metal and dielectric losses, $r(\omega)$ and $g(\omega)$ respectively, are purely real because the corresponding imaginary parts are absorbed by frequency-dependent PUL inductance and capacitance $L(\omega)$ and $C(\omega)$. For brevity, we will omit frequency arguments in these variables.

Thus, imaginary and real components in the power can be separated as follows:

$$G(i\omega) \approx e^{-i\omega l\sqrt{LC}[1+\frac{r(\omega)}{2i\omega L}+\frac{g(\omega)}{2i\omega C}]} = e^{-i\omega l\sqrt{LC}} e^{-\frac{1}{2}l\left(\sqrt{\frac{C}{L}}r(\omega)+\sqrt{\frac{L}{C}}g(\omega)\right)} \tag{19}$$

Magnitude of the propagation operator in (19) can be converted into Insertion Loss:

$$IL = -\frac{10}{\log(10)} l\left(\sqrt{\frac{C}{L}}r(\omega)+\sqrt{\frac{L}{C}}g(\omega)\right). \tag{20}$$

If there is a loss correction factor in $r(\omega)$, it should be visible on the insertion loss plot as a multiplier to the skin resistance. As implied by #6 and #7 in Table 1, the resistive part $r(\omega)$ has a multiplier $1+K_{0r}(\omega)-K_{0i}(\omega)$, whereas the corresponding contribution into an inductance gets the multiplier equal $1+K_{0r}(\omega)+K_{0i}(\omega)$. From here, we can represent frequency dependent inductance as $L(\omega)=L_\infty+(R_s/\sqrt{\omega})(1+K_{0r}(\omega)+K_{0i}(\omega))$, where L_∞ is a value of inductance at "infinity".

A non-causal roughness model applies an identical factor to both resistive and inductive contributions from skin impedance. That is, the resistive losses $r(\omega)$ are similar to causal case, but inductive component $L(\omega)=L_\infty+(R_s/\sqrt{\omega})(1+K_{0r}(\omega)-K_{0i}(\omega))$ is smaller because $K_{0i}(\omega)>0$. For convenience, we denote the common part of inductance that presents in both cases as $L_{cmn}(\omega)=L_\infty+(R_s/\sqrt{\omega})(1+K_{0r}(\omega))$. Then, inductance for causal and non-causal cases becomes $L_{cmn}(\omega)+(R_s/\sqrt{\omega})K_{0i}(\omega)$ and $L_{cmn}(\omega)-(R_s/\sqrt{\omega})K_{0i}(\omega)$ respectively.

Magnitude of the propagation operator, is it affected by non-causality?

When computing insertion loss in (20), resistive loss $r(\omega)$ is the same regardless of model causality. What changes is inductance. It becomes larger when using a causal model. Larger inductance will reduce the effect of resistive losses and increase conductive losses. However, resistive losses dominate at low frequency, and conductive at high frequency. That's why the model with causal roughness will show slightly less loss at low frequency but larger at high frequency. The variation of insertion loss can be estimated as:

$$\Delta IL = IL_{caus} - IL_{noncaus} \approx \frac{10}{\log(10)} l \frac{R_s K_{0i}}{L_{cmn}\sqrt{\omega}}\left(\sqrt{\frac{C}{L_{cmn}}}r(\omega)-\sqrt{\frac{L_{cmn}}{C}}g(\omega)\right). \tag{21}$$

The difference is very small because of the multiplier in changes its sign and remains close to zero.

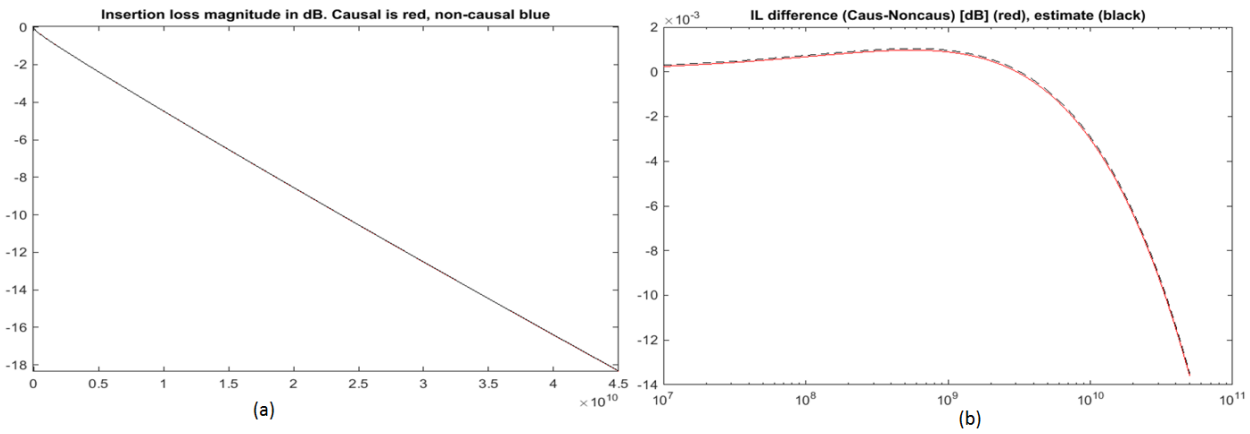

Figure 5. (a) IL plots for causal and non-causal models (red/blue), (b) the difference between IL dependencies: red – found directly from the extracted S-parameters, dashed blue – estimated.

In Figure 5 a, b, we compare insertion loss from S-parameters generated with causal and non-causal roughness models. Figure 5a shows that IL plots are practically identical. The difference is indeed very small, as seen in Figure 5b, and the sign changes at approximately 3GHz. Formula (21) gives very accurate estimate, shown by dashed line.

Propagation phase and phase delay

The first term in (19) describes the phase of the propagation function, which is $\varphi(\omega) = -\omega l\sqrt{LC}$. We can evaluate this value for causal and non-causal models at mid and high frequency (assuming that $\frac{R_s}{L(\omega)\sqrt{\omega}} << 1$) as $\varphi_{caus/noncaus}(\omega) = -\omega l\sqrt{L_{cmn}C}\sqrt{1 \pm \frac{R_s}{L_{cmn}\sqrt{\omega}}K_{0i}} \approx$ $-\omega l\sqrt{L_{cmn}C}\left(1 \pm \frac{R_s}{2L_{cmn}\sqrt{\omega}}K_{0i}\right)$. For causal model, we should take "+" in this expression. From here, the difference in phase becomes $\varphi_{caus}(\omega) - \varphi_{noncaus}(\omega) = -l\sqrt{\frac{C}{L_{cmn}}}R_s\sqrt{\omega}K_{0i}$, and the phase delay:

$$T_{ph\_caus}(\omega) - T_{ph\_noncaus}(\omega) = l\sqrt{\frac{C}{L_{cmn}}}R_s\frac{K_{0i}}{\sqrt{\omega}}. \quad (22)$$

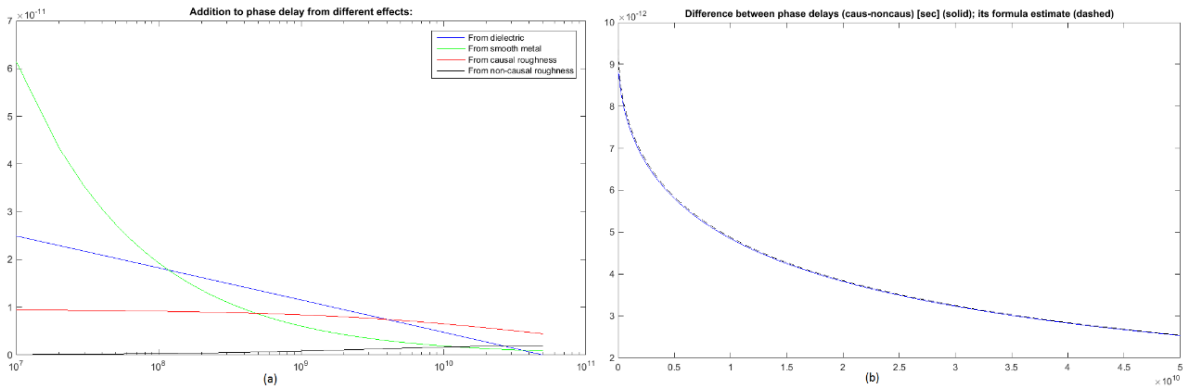

Figure 6. (a) Contribution into phase delay from different types of losses; (b) the difference in phase delay due to roughness causality: simulated (solid) and predicted by (22) (dashed)

Figure 6a shows contribution from different losses into the phase delay. A loss-less transmission line has constant phase and group delay. For a lossy line an additional delay decreases with frequency and approaches the value defined by capacitance and inductance at infinity. For a given test case, the largest addition comes from impedance of the smooth metal (green), which dominates at low frequency. It decreases approximately as $1/\sqrt{\omega}$, as relative contribution of inductance due to skin effect.

Next by importance comes additional delay caused by extra capacitance associated with dielectric loss (blue). This dependence practically repeats the real part of Djordjevic-Sarkar equation for relative permittivity of dielectric.

Contribution into phase delay from the causal roughness model (red) remains almost constant within wide range. At low frequency, we have $\sim\sqrt{\omega}$ increase of the factor $K_{0r}(\omega)+K_{0i}(\omega)$. Multiplied by an impedance of the smooth metal, also growing at this rate, it makes a linearly growing contribution that practically stays in constant proportion with ωL_∞ thus increasing an equivalent inductance and phase delay. Only at higher frequency, where blue curves in Figure 2b become flat, this factor settles and its relative contribution diminishes.

For non-causal model (black), the multiplier at inductive impedance $K_{0r}(\omega)-K_{0i}(\omega)$ is by orders smaller, and practically not visible. At higher frequency, the red curve in Figure 2b approaches blue, because imaginary part of the complex correction factor starts to go down and the lack of it becomes less visible. This is where contributions from causal and non-causal models converge.

Figure 6b illustrates the difference in phase delay caused by using causal model. Solid is simulated, while dashed is predicted by formula (22). The difference slowly decreases but remains considerable up to 50GHz. This is consistent with red/black curves in Figure 6a.

Characteristic impedance of the line

At sufficiently high frequency ($\frac{R_s}{L_{cmn}\sqrt{\omega}} << 1$), we have $Z_c(\omega) = \sqrt{\frac{i\omega L + r(\omega)}{i\omega C + g(\omega)}} =$ $\sqrt{\left[i\omega\left(L_{cmn} \pm \frac{R_s}{\sqrt{\omega}} K_{0i}\right) + r(\omega)\right] / \left[i\omega C + g(\omega)\right]}$. We choose "+" for causal and "-" for non-causal model. By assuming that losses are small and expanding the expression under square root, we find the difference:

$$Z_c(\omega) - Z_{nc}(\omega) \approx \frac{R_s}{\sqrt{L_{cmn} C}} \frac{K_{0i}}{\sqrt{\omega}}. \tag{23}$$

More accurate estimate is possible if we don't ignore losses but consolidate them in the denominator, as follows:

$$Z_c(\omega) - Z_{nc}(\omega) \approx \frac{i\sqrt{\omega} R_s K_{0i}}{Z_{PUL}(i\omega)} Z_c(\omega) = \frac{i\sqrt{\omega} R_s K_{0i}}{\sqrt{Y_{PUL}(i\omega) Z_{PUL}(i\omega)}}. \tag{24}$$

In this expression, the denominator depends on PUL conductance and impedance. It is mostly imaginary and grows linearly with frequency. Therefore, the surplus in characteristic impedance is mostly real, and decreases as $1/\sqrt{\omega}$.

Figure 7 shows the difference in characteristic impedance caused by model causality. Red and blue curves are real/imaginary parts of this difference found from two simulations. Green illustrates real part of the difference found by the simplified equation (23). Dashed black and cyan show real/imaginary parts of more accurate evaluation of this difference per equation (24). The latter perfectly matches numerical evaluation.

At low frequency the nominator in (24) grows linearly, the same as the denominator, thus making the difference approximately constant. At higher frequency, K_{0i} peaks, then starts decreasing; thus making this difference smaller. In our particular case the difference in characteristic impedance between causal and non-causal models is about 1% compared to ~50 Ohm characteristic impedance. But depending on line's parameters, it could be larger or smaller.

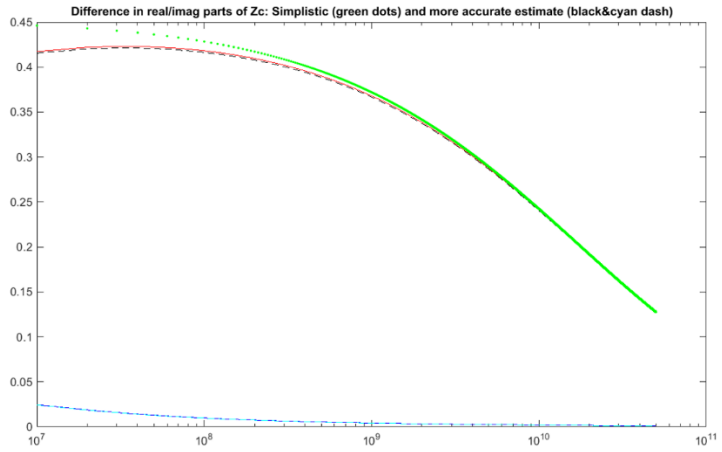

Figure 7. The difference in characteristic impedance of the line due to causality of the roughness model

V. Restoring causal correction factor from the loss factor given by a table

Sometimes material vendors describe loss correction factor by tabulated dependence $K_{loss}(\omega_n)$ given as (frequency, value) pairs. This dependence corresponds to #2 or #6 in Table 1; hence it is a difference between real and imaginary parts of the unknown complex multiplier $K(i\omega)$.

Since $K(i\omega)$ should be a causal dependence, it's tempting to represent it by a sum of simple rational components, for example as $K_0(i\omega) = A_\infty + \sum_{m=1}^{M} \frac{A_m}{1 + i\omega/\omega_m}$, then equate the table-given dependence, $K_{loss}(\omega_n) - 1$ to the difference between real and imaginary parts of this representation and then try to find the unknown coefficients. However, this approach fails in most cases because the task becomes ambiguous. Although we can restore a missing real (imaginary) part from a given imaginary (real) part, there is no single solution when restoring the two if we only know the difference between them.

As shown in Figure 8a, the real and imaginary parts of the fitted approximation to $K_0(i\omega)$ remain uncontrollable outside the data range, even though the loss factor is fitted accurately (Figure 8b). Note that both multipliers in Figure 8b decrease above ~10GHz, which doesn't match our expectations.

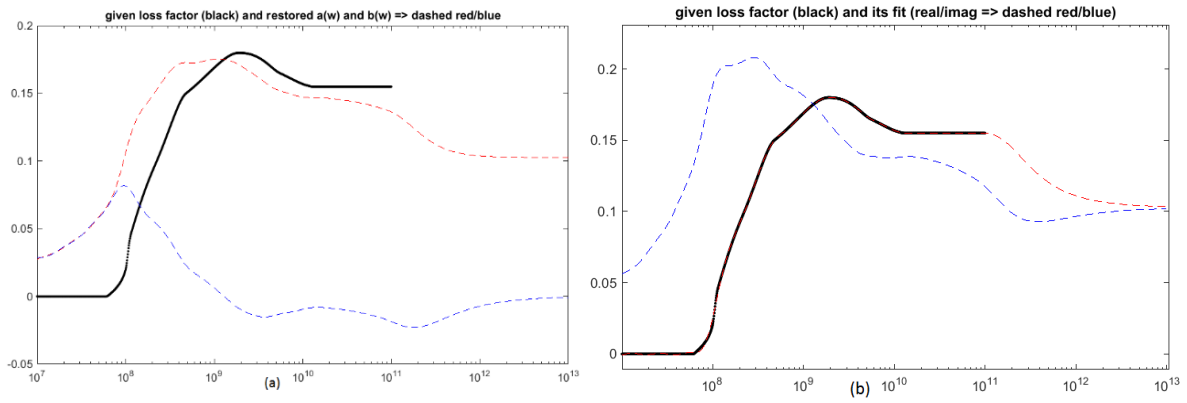

Figure 8. (a) Given loss factor (black), real and imaginary parts of the fit (red/blue) whose difference approximates the loss factor; (b) fitted loss (red) and inductance (blue) correction factors

The proper way is to work with complex impedance, for which we can find real part. For example, a normalized surplus of PUL impedance can be represented as

$$Z_{00}(i\omega) = Z_0(i\omega)/R_s = \sqrt{\omega}\{[K_{0r}(\omega) - K_{0i}(\omega)] + i[K_{0r}(\omega) + K_{0i}(\omega)]\},$$

assuming the complex factor $K_0(i\omega) = K_{0r}(\omega) + iK_{0i}(\omega)$, $K_{0r}(0) = K_{0i}(0) = 0$. Therefore real part of the surplus impedance should interpolate values $\mathrm{Re}\, Z_{00}(i\omega_n) \approx \sqrt{\omega_n}[K_{0r}(\omega_n) - K_{0i}(\omega_n)] = \sqrt{\omega_n}[K_{loss}(\omega_n) - 1]$. Since $Z_{00}(i\omega)$ is causal, it can be approximated e.g. by a rational fraction expansion of the form:

$$Z_{00}(i\omega) = A_\infty + \sum_{m=1}^{M} \frac{A_m}{1 + i\omega/\omega_m} = A_\infty + \sum_{m=1}^{M} \frac{A_m}{1 + (\omega/\omega_m)^2} + i\sum_{m=1}^{M} \frac{-(\omega/\omega_m)A_m}{1 + (\omega/\omega_m)^2}. \qquad (25)$$

To simplify the task, we can choose a set of M (typically 15…30) real poles ω_m distributed linearly or logarithmically within the range of interest, and reduce the problem to finding the coefficients only. Note that since $Z_{00}(0) = 0$, we should require that $A_\infty = -\sum_{m=1}^{M} A_m$ therefore (25) becomes

$$Z_{00}(\omega) = -\sum_{m=1}^{M} \frac{A_m(\omega/\omega_m)^2}{1 + (\omega/\omega_m)^2} - i\sum_{m=1}^{M} \frac{(\omega/\omega_m)A_m}{1 + (\omega/\omega_m)^2}. \qquad (26)$$

Obviously, we can find factors A_m by equating real part of (26) to $\sqrt{\omega_n}[K_{loss}(\omega_n) - 1]$ for a given set of frequency samples and solving the linear system e.g. by singular value decomposition method. For better accuracy, we can also normalize both parts of equation on $\sqrt{\omega}$. After solving equation for A_m, unknown term $\sqrt{\omega}\{[K_{0r}(\omega) + K_{0i}(\omega)]$ can be restored as imaginary part of (26).

Now, that we have approximation for real and imaginary parts $T_r(\omega) = K_{0r}(\omega) - K_{0i}(\omega)$ and $T_i(\omega) = K_{0r}(\omega) + K_{0i}(\omega)$, we can find $K_{0r}(\omega)$ and $K_{0i}(\omega)$ as

$$K_{0r}(\omega) = \frac{1}{2}[T_r(\omega) + T_i(\omega)],\ K_{0i}(\omega) = \frac{1}{2}[T_i(\omega) - T_r(\omega)]. \tag{27}$$

Here, the functions $T_r(\omega) = -\sum_{m=1}^{M} \frac{A_m \omega \sqrt{\omega}/\omega_m^2}{1+(\omega/\omega_m)^2}$ and $T_i(\omega) = -\sum_{m=1}^{M} \frac{(\sqrt{\omega}/\omega_m)A_m}{1+(\omega/\omega_m)^2}$ are fully defined by the chosen set of poles ω_m and found coefficients A_m. The complex correction factor of interest becomes a combination of real/imaginary parts from (27).

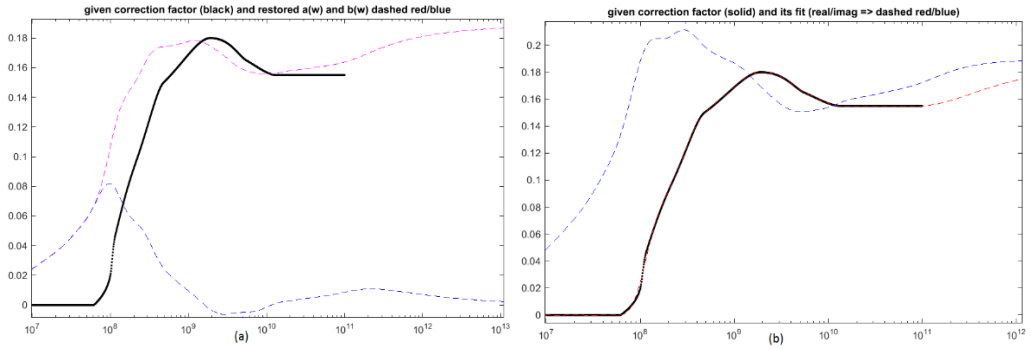

Figure 9. Given loss factor (black), real and imaginary parts of the restored complex correction factor (red/blue) (a). Loss (red) and inductance correction factors (blue), restored by fit (b)

Unlike Figure 8, here we observe more stable behavior of the correction factors while ensuring sufficiently accurate fit of the loss factor.

VI. Cannonball-Huray Model

Building upon the work already done by Huray [3], the Cannonball model is used to determine the radius and base area parameters in the original Huray model. As opposed to the stacked sphere approximation using scanning electron microscopy (SEM) data, the Cannonball model determines the exact sphere radius and flat base area based solely on roughness parameters published in manufacturers' data sheets.

Using the principle of stacking cannonballs, 14 uniform spheres, with radius (r), are stacked in a pyramidal structure, on a flat tile base, with an area A_{flat}, as illustrated in Figure 10

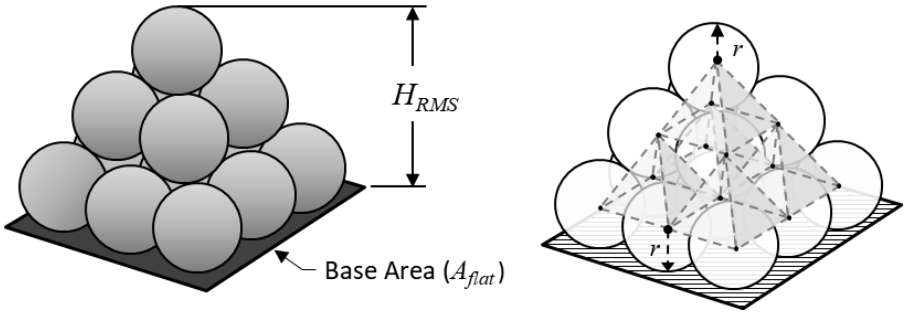

Figure 10. Cannonball model showing 9 spheres on the base row; 4 spheres in the middle row; and a single sphere on top. Five pyramid lattice structures join all 14 sphere centers as shown.

If we could peer inside the stack of spheres, and imagine 5 pyramids in a stacked lattice structure connecting the centers of all 14 spheres the radius can be easily determined by simple geometry and algebra.

Given the total height of the cannonball stack is equal to H_{RMS}, then from method described in [11], determining the radius of a single sphere (r), from 10-point mean roughness (R_z) parameter from data sheet, can be further simplified and approximated by

$$r \approx 0.06 R_z \qquad \text{(CH-1)}$$

And therefore the area of the flat tile base A_{flat} is

$$A_{flat} = 36r^2 . \qquad \text{(CH-2)}$$

Since the Cannonball-Huray model assumes 14 equally sized spheres stacked in a cannonball stack, and the nodule treatment is applied to a perfectly flat surface, the original Huray model is simplified and thus the power loss correction factor, $K_{CBH}(f)$, can be determined by [11]:

$$K_{CBH}(f) \approx 1 + 84\left(\frac{\pi r^2}{A_{flat}}\right) \div \left(1 + \frac{\delta(f)}{r} + \frac{(\delta(f))^2}{2r^2}\right) \qquad \text{(CH-3)}$$

where r is sphere radius in meters; $\delta(f)$ is skin depth, as a function of frequency, in meters, A_{flat} is an area of a single square flat tile base in sq. meters.

Case Study

To test the accuracy of the model, measured data, from a CMP-28 Channel Modeling Platform, courtesy of [9], 10] was used for model validation. The extracted de-embedded S-parameter data was computed from 2 inch and 8 inch single-ended stripline traces.

The printed circuit board (PCB) was fabricated with Isola [16] FR408HR 3313 dielectric and 1 oz. MLS Grade 3, controlled elongation reverse treated foil (RTF), from Oak-mitsui [17]. The data sheet and PCB design parameters are summarized in Table 2.

Dielectric constant, D_k dissipation factor, D_f, and R_z are the values as reported in the respective manufactures' data sheets. An oxide or micro-etch treatment is usually applied to the copper surfaces prior to final PCB lamination. The etch treatment creates a surface full of micro-voids which follows the underlying rough profile and allows the resin to squish in and fill the voids providing a good anchor. Because some of the copper is typically removed during the micro-etch treatment, the published roughness parameter of the matte side was reduced by nominal 50 μin (1.27 μm) for a new thickness of 4.445μm, used for matte side correction factor analysis.

Table 2 CMP-28 Test Board and Data Sheet Parameters

Parameter	Value
D_k Core/Prepreg @ f_o	3.68/3.62@1GHz
D_f Core/Prepreg @ f_o	0.0087/0.0089 @ 1GHz
R_z Drum side	3.048 μm
R_z Before Micro-etch-Matte side	5.715 μm
R_z After 50 μin (1.27 μm) Micro-etch treatment - Matte side	4.445 μm
Trace Thickness, *t*	1.25 mils (31.73 μm)
Trace Etch Factor	60 deg taper
Trace Width, w	11 mils (279.20 μm)
Core thickness, H1	12 mils (304.60 μm)
Prepreg thickness, H2	10.6 mils (269.00 μm)
De-embedded trace length	6.00 in (15.24 cm)

In [12], the authors observed an increase in phase delay proportional to roughness profile and dielectric material thickness. In [13] it was shown that the increased phase delay can be partly attributed to increased capacitance due to surface roughness. Because laminate suppliers' data sheets typically report D_k as the value measured in a production environment, it does not guarantee the values are correct for design applications. In most cases the value published is lower that what is finally measured after the PCB has been fabricated.

If the roughness of copper foil and dielectric constant from manufacturers' data sheets are known, then the increase in effective dielectric constant (D_{keff}) can be approximated by [13]:

$$D_{keff} \approx \frac{t_{diel}}{\left(t_{diel} - 2R_z\right)} \times D_k \qquad \text{(CH-4)}$$

where t_{diel} *is* the dielectric material thickness, R_z is the 10-point mean roughness, and D_k is the dielectric constant for as published in respective manufacturers' data sheets.

From Table 2 and by applying (CH-4), D_{keff} of core and prepreg due to roughness were determined as

$$D_{keff\_core} = \frac{H_{smooth}}{\left(H_{smooth} - 2R_z\right)} \times D_{k\_core} = \frac{304.6\mu m}{\left(304.6\mu m - 2 \times 3.048\mu m\right)} \times 3.68 = 3.755@1GHz$$

$$D_{keff\_prepreg} = \frac{H_{smooth}}{\left(H_{smooth} - 2R_z\right)} \times D_{k\_prepreg} = \frac{269\mu m}{\left(269\mu m - 2 \times 4.445\mu m\right)} \times 3.62 = 3.744@1GHz$$

A modified version of Mentor HyperLynx [14] was used to include causal/non-causal conductor models and Cannonball-Huray correction factors for matte and drum sides of the foil based on (CH-3). Corrected D_{keff} for core and prepreg, based on (CH-4), were used while D_f for core and prepreg remained unchanged from Table 2.

Keysight ADS [15] was used for simulation analysis and comparison to measured data. Frequency domain results are presented in Figure 11. The left graph shows measured insertion loss of a de-embedded 6 inch stripline trace vs causal and non-causal models. As can be seen, there is virtually no difference between causal and non-causal model simulations.

The right graph of Figure 11 shows measured phase delay vs causal and non-causal models. The non-causal model is consistent with phase delay compensation results published in [13]. But when the causal version of conductor roughness model was applied we observe that simulated phase delay matches measured phase delay almost exactly. This is remarkable, considering there was no additional tuning or curve of fitting parameters from manufacturers' data sheet values.

Figure 12 shows simulated vs measured results. Time delay transmission (TDT) impulse response is shown on the left graph while time domain reflected (TDR) impedance is shown on right graph. As can be seen, there is excellent correlation between causal models and measured data for both graphs. Also worth noting the causal model has higher characteristic impedance and is a better fit to measured results compared to non-causal model as expected.

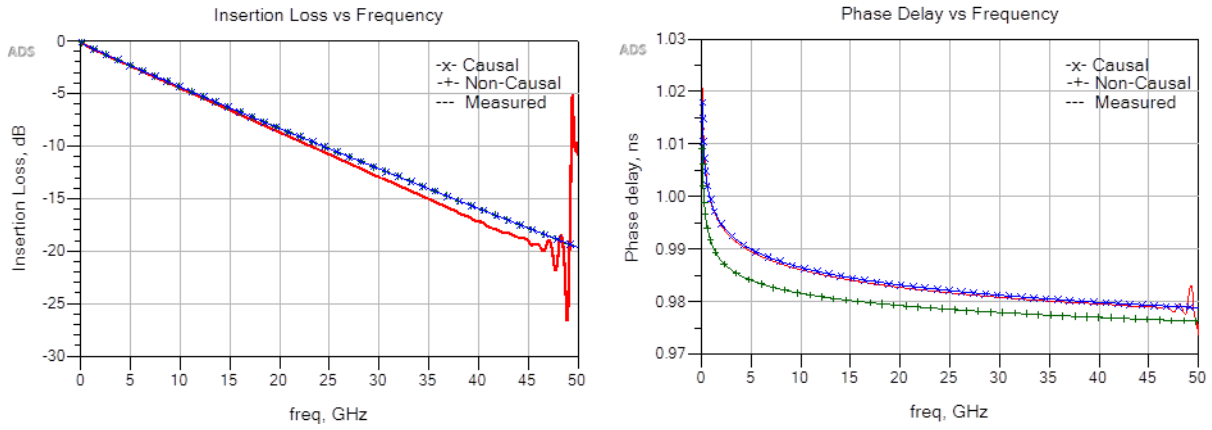

Figure 11. Causal / non-causal vs measured insertion loss (IL) (left) and phase delay (right).

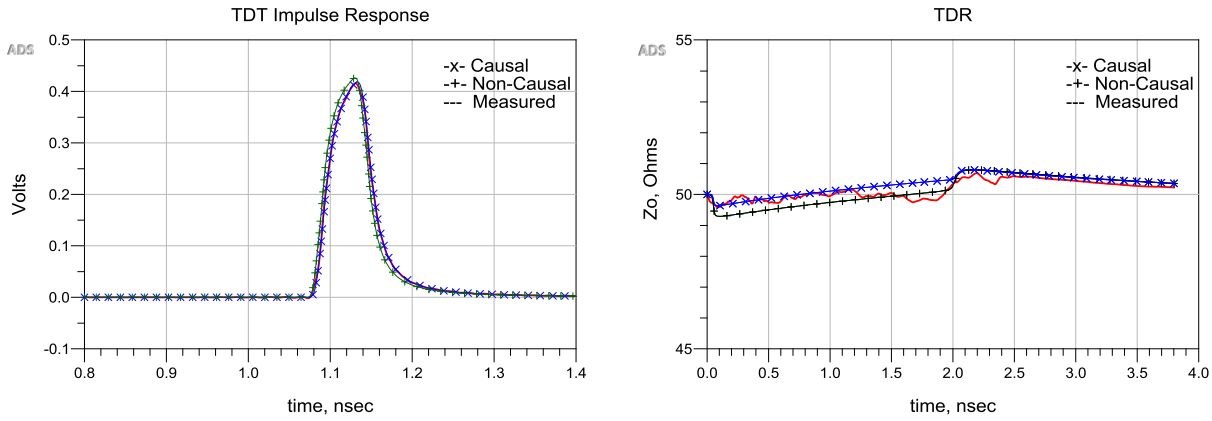

Figure 12. Causal / non-causal vs measured time domain transmission (TDT) impulse response (left) and time domain reflected (TDR) response (right).

Conclusion

In this paper, we presented a causal version of the roughness correction factor associated with certain loss models. Although the Hammerstad and Cannonball-Huray models have been considered in detail, the method described in this work also applies to other models, given by formulas or tables.

We considered the impact created by causality of metal roughness on the characteristics of transmission lines. The effect it makes on insertion loss, phase delay and characteristic impedance was described analytically as functions of PUL parameters. These formula estimates show perfect agreement with simulated results.

We also demonstrated that phase delay and characteristic impedance considerably increased, compared to the case of using a non-causal, real-value correction multiplier. Simulated results appear in a perfect agreement with measured characteristics of the example case study.

In the end, we note that causal and non-causal models of metal roughness are not just two versions of the same model. Causal models could be wrong in many ways, but at least they have a potential to correctly describe the relation between the current density and the electric field on metal's surface, which is a causal function. A non-causal model, on the other hand, is always wrong, and it's only a question of how large the error it brings into simulation.

References

[1] S. Hall, S. Pytel, P. Huray et al. "Multigigahertz causal transmission line modeling methodology using a 3-D hemispherical surface roughness approach," IEEE Trans. on Microwave Theory and Techniques, v.55, No.12, 2007

[2] S. Hall, H. Heck, "Advanced signal integrity for high speed digital designs," John Willey & Sons Inc., Hoboken, NJ, 2009.

[3] P. Huray, "The foundations of signal integrity," John Willey & Sons Inc., Hoboken, NJ, 2009.

[4] E. Bogatin, D. DeGroot, P. Huray, and Y. Shlepnev, "Which one is better? Comparing options to describe frequency dependent losses," DesignCon 2013.

[5] Appendix E. "Causal relationship between skin effect resistance and internal inductance for rough conductors," – in [2].

[6] E. Bracken, "A causal Huray model for surface roughness", DesignCon 2012.

[7] A. Djordjevic, R. Biljie, V. Likar-Smiljanic, T. Sarkar, "Wideband frequency domain characterization of FR-4 and time domain causality", IEEE Trans. on EMC, vol.43, No.4, 2001.

[8] Y. Shlepnev, "Modeling frequency-dependent dielectric loss and dispersion for multigigabit data channels", Simbeor Application Note 2008.

[9] Simberian Inc., 3030 S Torrey Pines Dr. Las Vegas, NV 89146, USA. URL: http://www.simberian.com/

[10] Wild River Technology LLC 8311 SW Charlotte Drive Beaverton, OR 97007. URL: https://wildrivertech.com/

[11] B. Simonovich, "Practical model of conductor surface roughness using cubic close-packing of equal spheres", EDICon 2016

[12] A. F. Horn, J. W. Reynolds and J. C. Rautio, "Conductor profile effects on the propagation constant of microstrip transmission lines," Microwave Symposium Digest (MTT), 2010 IEEE MTT-S International, Anaheim, CA, 2010, pp. 1-1.doi: 10.1109/MWSYM.2010.5517477

[13] B. Simonovich, "A practical method to model effective permittivity and phase delay due to conductor surface roughness", DesignCon 2017

[14] Mentor Hyperlynx [computer software] URL: https://www.mentor.com/pcb/hyperlynx/

[15] Keysight Advanced Design System (ADS) [computer software], (Version 2016). URL: http://www.keysight.com/en/pc-1297113/advanced-design-system-ads?cc=US&lc=eng

[16] Isola Group S.a.r.l., 3100 West Ray Road, Suite 301, Chandler, AZ 85226. URL: http://www.isola-group.com/
[17] Oak-mitsui 80 First St, Hoosick Falls, NY, 12090. URL: http://www.oakmitsui.com/pages/company/company.asp

Appendix A. Derivation of causal correction factor for Huray-Cannonball model

Using the expression (13) describing loss correction factor together with (6), we find the resistive part of the additional impedance due to metal roughness be

$$Z_{0r}(x) = \frac{x\sqrt{x}}{x+\sqrt{2x}+1} R_s . \qquad \text{(A1)}$$

This must be a real part of the complex frequency-dependent impedance, which is assumed causal. At this point, we'd like to restore unknown imaginary part of the complex impedance by applying K-K integral transformation. Unfortunately, these integrals are defined for the functions that disappear at infinity, but (A1) grows asymptotically as $\sqrt{x}$. One way to remove this obstacle is to consider an equivalent complex inductance, defined by (11). When we divide complex impedance on complex frequency, a real part of the first is converted into imaginary part of the complex inductance:

$$L_{0i}(x) = -\frac{\sqrt{x}}{x+\sqrt{2x}+1} R_s . \qquad \text{(A2)}$$

Since complex inductance is a causal function, too, and disappears at infinity, we can apply K-K integral of the form

$$\mathrm{Re}U(x) - U_\infty = -\frac{2}{\pi} v.p.\int_0^\infty \frac{y\,\mathrm{Im}U(y)}{y^2-x^2} dy \qquad \text{(A3)}$$

to restore unknown real part of the causal function from known imaginary. Substituting (A2) into this integral, we get

$$Q_r(x) = L_{0r}(x)/R_s = \frac{2}{\pi} v.p.\int_0^\infty \frac{y\sqrt{y}}{(y^2-x^2)(y+\sqrt{2y}+1)} dy . \qquad \text{(A4)}$$

With $t=\sqrt{y}$, (A4) becomes $Q_r(x) = \frac{2}{\pi}\int_0^\infty \frac{2t^4 dt}{(t^4-x^2)(t^2+t\sqrt{2}+1)}$, whose integrand can be represented as

$$\frac{2t^4}{(t^4-x^2)(t^2+t\sqrt{2}+1)} = \frac{2}{1+x^2}\left[\frac{1}{t^2+t\sqrt{2}+1} + x^2\frac{t^2-t\sqrt{2}+1}{t^4-x^2}\right].$$

By substituting $u = t+1/\sqrt{2}$, integral from the first summand in brackets becomes

$$\int_0^\infty \frac{dt}{t^2+t\sqrt{2}+1} = \int_{1/\sqrt{2}}^\infty \frac{du}{u^2+\frac{1}{2}} = \sqrt{2}\arctan(u\sqrt{2})\Big|_{1/\sqrt{2}}^\infty = \frac{\pi\sqrt{2}}{4}.$$

Second integral yields $x^2\int_0^\infty \frac{t^2-t\sqrt{2}+1}{t^4-x^2}dt = \frac{\pi}{4}\sqrt{x}(x-1)$. To calculate it, note that the odd part of the integrand gives zero: $\int_0^\infty \frac{tdt}{t^4-x^2} = \frac{1}{2}\int_0^\infty \frac{du}{u^2-x^2} = 0$, and remaining integral may be calculated using residues:

$$\int_0^\infty \frac{t^2+1}{t^4-x^2}dt = \frac{1}{2}\int_{-\infty}^\infty \frac{t^2+1}{t^4-x^2}dt = 2\pi i\,\mathrm{Res}(f(t), i\sqrt{x}) = 2\pi i\frac{t^2+1}{4t^3}\Big|_{t=i\sqrt{x}} = \frac{\pi(x-1)}{4x\sqrt{x}}.$$

Here, integrals at small semicircles around $t=\pm\sqrt{x}$ cancel each other, so we consider the only remaining pole in the upper half-plane.

Finally, collecting the pieces of the integral together, we get $Q_r(x) = \frac{\sqrt{2}+\sqrt{x}(x-1)}{1+x^2}$, which can be simplified into

$$L_{0r}(x)/R_s = Q_r(x) = \frac{\sqrt{x}+\sqrt{2}}{x+\sqrt{2x}+1}. \qquad \text{(A5)}$$

From (A2), (A5), we compose the complex inductance as

$$L_0(ix)/R_s = \frac{\sqrt{2}+\sqrt{x}}{x+\sqrt{2x}+1} - i\frac{\sqrt{x}}{x+\sqrt{2x}+1}. \qquad \text{(A6)}$$

As a frequency response of a causal function, (A6) should be a real function of complex frequency $s=ix$. To find this form, we use $x=s/i=-is$. Since integral is taken over positive half axis, we assume that $\mathrm{Im}\{s\}\ge 0$. Therefore, square roots are related as $\sqrt{s}=\sqrt{ix}=\frac{1}{\sqrt{2}}(1+i)\sqrt{x}$ hence we should replace $\sqrt{x}$ by $\sqrt{x}=\frac{1}{\sqrt{2}}(1-i)\sqrt{s}$. With these substitutions in (A6) the complex terms vanish and after a few elementary transformations we arrive to:

$$L_0(ix)/R_s = \frac{\sqrt{2}}{1+\sqrt{s}} = \frac{\sqrt{2}}{1+\sqrt{ix}}. \qquad \text{(A7)}$$

From (A7), we can find complex impedance, added due to metal roughness as

$$Z_0(ix)/R_s = (ix)L_0(ix)/R_s = \frac{\sqrt{2}(ix)}{1+\sqrt{ix}} = \frac{\sqrt{2}s}{1+\sqrt{s}}. \qquad \text{(A8)}$$

Finally, considering (A8) together with (2) and (7), we find the complex roughness correction factor as

$$K_0(ix) = \frac{\sqrt{ix}}{1+\sqrt{ix}} = \frac{\sqrt{s}}{1+\sqrt{s}}. \qquad \text{(A9)}$$

This result agrees with the one from [6].

Appendix B. Derivation of causal correction factor for Hammerstad model

The main steps are same as in Appendix A for the Cannonball-Huray model. From (16) and (6), we get

$$Z_{0r}(x) = \frac{2}{\pi}\sqrt{x}\arctan(x)R_s. \qquad \text{(B1)}$$

From where imaginary part of the additional complex inductance becomes:

$$L_{0i}(x) = -\frac{2}{\pi}\frac{1}{\sqrt{x}}\arctan(x)R_s. \qquad \text{(B2)}$$

With that, integral in K-K relation acquires the form:

$$Q_r(x) = L_{0r}(x)/R_s = \left(\frac{2}{\pi}\right)^2 v.p.\int_0^\infty \frac{\sqrt{y}\arctan(\alpha y)}{y^2-x^2}dy \qquad \text{(B3)}$$

where parameter α equals 1. It is convenient however to find the derivative of (B3) by this parameter first:

$$\frac{\partial Q_r(x,\alpha)}{\partial\alpha} = \left(\frac{2}{\pi}\right)^2\int_0^\infty \frac{y\sqrt{y}dy}{(y^2-x^2)(1+\alpha^2y^2)} = \left(\frac{2}{\pi}\right)^2\int_{-\infty}^\infty \frac{t^4dt}{(t^4-x^2)(1+\alpha^2t^4)}.$$

This integral may be taken analytically, but the easier way is to use a contour integral in the upper half-plane, which results in

$$\frac{\partial Q_r(x,\alpha)}{\partial\alpha} = \frac{2}{\pi}\left(\sqrt{\frac{2}{\alpha}}\frac{1}{1+\alpha^2x^2} - \frac{\sqrt{x}}{1+\alpha^2x^2}\right). \qquad \text{(B4)}$$

Now we need to integrate it by α. With $\alpha = t^2$, integral from the first summand in (B4) becomes

$$Q_r^{(1)}(x,\alpha) = \frac{2}{\pi}\int\sqrt{\frac{2}{\alpha}}\frac{d\alpha}{1+\alpha^2x^2} = \frac{4\sqrt{2}}{\pi}\int\frac{dt}{1+x^2t^4}.$$

This integral can be found using the result e.g. from H. Dwight, Table of integrals and other mathematical data, McMillan, 1961:

$$\int\frac{dt}{t^4+m^4} = \frac{1}{4\sqrt{2}m^3}\ln\frac{t^2+\sqrt{2}mt+m^2}{t^2-\sqrt{2}mt+m^2} + \frac{1}{2\sqrt{2}m^3}\arctan\frac{\sqrt{2}mt}{m^2-t^2}.$$

In our case $m^2 = 1/x$ and $t^2 = \alpha$, therefore

$$Q_r^{(1)}(x,\alpha) = \frac{4\sqrt{2}}{\pi x^2}\int\frac{dt}{(1/x)^2+t^4} = \frac{2}{\pi\sqrt{x}}\left[\frac{1}{2}\ln\frac{1+\sqrt{2\alpha x}+\alpha x}{1-\sqrt{2\alpha x}+\alpha x} + \arctan\frac{\sqrt{2\alpha x}}{1-\alpha x}\right].$$

Integral from the second summand in (B4) is simple:

$$Q_r^{(2)}(x,\alpha) = -\frac{2}{\pi}\sqrt{x}\int \frac{d\alpha}{1+\alpha^2 x^2} = -\frac{2}{\pi\sqrt{x}}\arctan(\alpha x).$$

Now, substituting $\alpha = 1$, and collecting the pieces together, we get:

$$Q_r(x) = \frac{2}{\pi\sqrt{x}}\left[\frac{1}{2}\ln\frac{1+\sqrt{2x}+x}{1-\sqrt{2x}+x} + \arctan\frac{\sqrt{2x}}{1-x} - \arctan(x)\right]. \qquad \text{(B5)}$$

With that, the complex addition to inductance due to roughness becomes

$$L_0(ix)/R_s = \frac{2}{\pi\sqrt{x}}\left[\frac{1}{2}\ln\frac{1+\sqrt{2x}+x}{1-\sqrt{2x}+x} + \arctan\frac{\sqrt{2x}}{1-x} - \arctan(x)\right] - i\frac{2}{\pi}\frac{1}{\sqrt{x}}\arctan(x). \qquad \text{(B6)}$$

Similar to what we did in Appendix A, by substitution $x = -is$ and $\sqrt{x} = \frac{1}{\sqrt{2}}(1-i)\sqrt{s}$, we convert (B6) into real function of complex frequency:

$$L_0(s)/R_s = \frac{\sqrt{2}}{\pi\sqrt{s}}\left[\log\frac{1+\sqrt{s}}{1-\sqrt{s}} - \log\frac{1+s}{1-s} + 2\arctan(\sqrt{s})\right]. \qquad \text{(B7)}$$

Then, find complex impedance

$$Z_0(s)/R_s = sL_0(s)/R_s = \frac{\sqrt{2s}}{\pi}\left[\log\frac{1+\sqrt{s}}{1-\sqrt{s}} - \log\frac{1+s}{1-s} + 2\arctan(\sqrt{s})\right] \qquad \text{(B8)}$$

And, finally, the complex factor

$$K_0(s) = Z_0(s)/Z_{smooth}(s) = \frac{1}{\pi}\left[\log\frac{1+\sqrt{s}}{1-\sqrt{s}} - \log\frac{1+s}{1-s} + 2\arctan(\sqrt{s})\right]. \qquad \text{(B9)}$$